Nanoscale
Advances

PAPER

View Article Online
View Journal | View Issue

Cite this: *Nanoscale Adv.*, 2025, 7, 5658

Bottom-up sono-enzymatic approach to build antimicrobial and antifouling nano-enabled coatings on urinary catheters

Antonio Puertas-Segura,[a] Leonardo Martín Pérez,[a] Paul Savage,[b] Kristina Ivanova,[a] Gianluca Ciardelli[c] and Tzanko Tzanov*[a]

Received 12th June 2025
Accepted 4th August 2025

DOI: 10.1039/d5na00577a

rsc.li/nanoscale-advances

In this work, an antifouling and antibacterial nano-enabled coating for urinary catheters was synthesised using a bottom-up sono-enzymatic approach. Ceragenin CSA-131, an antimicrobial peptide, and lauryl gallate were nanoformulated into colloidal nanoparticles using high-intensity ultrasound. The obtained nanoparticles (GaCeNPs) were sonochemically deposited, together with sulfobetaine methacrylate (SB), and grafted enzymatically onto APTES-aminated silicone catheter material using laccase. Simultaneously, laccase-oxidised phenolic groups on GaCeNPs mediated the *in situ* radical polymerisation of the zwitterionic vinyl moieties into polysulfobetaine yielding a functional GaCeNPs_pSB coating. This coating effectively suppressed non-specific protein adsorption, as shown by reduced attachment of FITC-labelled bovine serum albumin, and achieved up to 3-log reduction in the growth of planktonic *E. coli* and *S. aureus* after 24 h. Contact angle measurements confirmed surface hydrophilicity (≈85°) of GaCeNPs_pSB-coated silicone for at least 7 days. Biofilm formation on Foley catheters functionalised with GaCeNPs_pSB was reduced by 70% upon incubation for a week in an artificial bladder model with continuous recirculation of infected urine. No adverse effects on fibroblast viability were observed over the same period of time in contact with the coated silicones, demonstrating their excellent biocompatibility (>90%). Altogether, this sono-enzymatically engineered, bio-based coating offers a promising strategy to reduce bacterial colonisation and biofilm formation on urinary indwelling devices and consequently the risk of infection in catheterised patients.

1. Introduction

Urinary tract infections associated with catheter use (*i.e.*, CAUTIs) are a major clinical concern and a key driver for developing advanced antimicrobial coatings on indwelling medical devices.[1,2] CAUTIs account for nearly 40% of all hospital-acquired infections, contributing to substantial morbidity and healthcare costs. Fitting of catheters facilitates microbial colonisation by enabling bacterial access to the patient's urinary tract through both extraluminal and intraluminal routes, even when closed drainage systems and aseptic protocols are routinely employed. Bacterial adhesion to catheter surfaces begins within hours, forming initial single-species biofilms that can develop into complex, antibiotic-resistant multispecies communities. These biofilms contribute to infections in up to 50% of patients during a typical 7-day catheterisation and often necessitate repeated catheter replacement and intensive antimicrobial therapy. Such interventions increase patient discomfort and drive the emergence of antimicrobial resistance, a major healthcare challenge.[3–5]

Silicone is the most widely employed material for manufacturing of urinary catheters due to its biocompatibility and reduced risk of allergic reactions, though it still fails to prevent microbial biofilm formation.[3] This has prompted the development of multifunctional surface coatings with both antibacterial and antifouling protection.[1,2,6,7] For this purpose, waterborne sonochemical functionalisation of polymer surfaces stands out as an environmentally friendly method for immobilisation of bioactive compounds. Our group has previously developed a laccase-assisted strategy to engineer phenolic–zwitterionic coatings on silicone urinary catheters. This approach enabled the covalent grafting of antifouling zwitterionic moieties onto aminated silicone surfaces through enzymatic phenol oxidation and *in situ* radical polymerisation.[8] While the initial system employed simple phenolic precursors such as gallic acid, subsequent optimisation included the use of silver-loaded phenolated lignin nanoparticles, which enhanced antimicrobial efficacy.[2] However, concerns regarding silver cytotoxicity and environmental accumulation due to medical

---

[a] Grup de Biotecnologia Molecular i Industrial, Departament d'Enginyeria Química, Universitat Politècnica de Catalunya (UPC-BarcelonaTech), Terrassa, Spain. E-mail: tzanko.tzanov@upc.edu

[b] Department of Chemistry and Biochemistry, Brigham Young University, Provo, USA

[c] Department of Mechanical and Aerospace Engineering, Politecnico di Torino, Torino, Italy

materials' disposal,[9] justify the transition toward metal-free, fully organic alternatives.

In this work, we report a refined, ultrasound-assisted bottom-up coating strategy for functionalisation of urinary catheters that combines laccase-mediated covalent grafting of antibacterial nanoparticles with *in situ* initiated radical polymerisation of a biocompatible zwitterionic methacrylate for antifouling, yielding a dual-functional surface. First, nanoparticles composed of lauryl gallate, an ester derivative of gallic acid, and ceragenin CSA-131, a cholic acid-based antimicrobial peptide,[10,11] were prepared using ultrasonic emulsification. Lauryl gallate contributes antioxidant and antibiofilm properties[12,13] and provides phenolic moieties that serve as reactive sites for laccase-mediated anchoring onto aminated silicone surfaces. Concurrently, CSA-131 imparts non-specific bactericidal activity through membrane disruption and induction of oxidative stress.[14,15] These nanoparticles (named GaCeNPs) were enzymatically grafted onto silicone surfaces that were plasma-preactivated and subsequently aminated. Furthermore, oxidised phenolic groups initiated the *in situ* radical polymerisation of sulfobetaine methacrylate (SB), resulting in a covalently bonded poly(sulfobetaine) (pSB) layer. The polyzwitterionic nano-enabled coating confers antifouling behaviour to the silicone materials by preventing non-specific adsorption of proteins and bacterial adhesion. Its antibacterial and antibiofilm efficacy was challenged against *E. coli* and *S. aureus*, clinically relevant CAUTI pathogens,[16] under both static and dynamic conditions in an artificial bladder model with continuous recirculation of infected urine. In parallel, the durability of the antibiofilm effect and biocompatibility of the nanocomposite coating was assessed over a week as a necessary step preceding further pre-clinical and clinical validations.

2. Experimental section

2.1 Materials

Polydimethylsiloxane (PDMS) urinary (Foley) catheters (16 French) and flat sheets of the same material were supplied by Degania Silicone Ltd (Israel). Ceragenin CSA-131 was synthesised *via* a cholic acid scaffolding approach, as previously reported.[17] Ethanol was purchased from Scharlab (Spain). Acetic acid, sodium acetate, dimethyl sulfoxide (DMSO), lauryl gallate, (3-aminopropyl) triethoxysilane (APTES), Tween® 80, phosphate-buffered saline (PBS), Muller-Hinton broth (MHB), tryptic soy broth (TSB), sulfobetaine methacrylate (SB), Baird-Parker agar, coliform agar, Dulbecco's modified Eagle's medium (DMEM), sodium dodecyl sulphate (SDS), fluorescein isothiocyanate-labelled bovine serum albumin (FITC-BSA), 2,2-diphenyl-1-picrylhydrazyl (DPPH), crystal violet and XTT cell proliferation kit II were purchased from Sigma-Aldrich (Spain). AlamarBlue cell viability reagent, and Live/Dead BacLight kit (L7012) were obtained from Invitrogen (Spain). Commercial laccase Novozym® 51003 from *Myceliophthora thermophila* (EC 1.10.3.2) was provided by Novozymes Spain S.A. (Spain). *Staphylococcus aureus* (ATCC 25923), *Escherichia coli* (ATCC 25922) and human fibroblast (ATCC-CRL-4001, BJ-5ta) cells were obtained from the American Type Culture Collection (ATCC® LGC Standards, Spain).

2.2 Synthesis and characterisation of GaCeNPs

Initially, 14 mL of a 0.02% (w/v) lauryl gallate solution in ethanol were mixed with 1 mL of a 100 mg per mL ceragenin CSA-131 dissolved in DMSO. The resulting mixture was combined in a 1 : 1 ratio with a 1% (v/v) aqueous solution of Tween® 80 and sonicated for 6 min at 20 °C (20 kHz, 35% amplitude) using a titanium horn ultrasonic processor (VCX750, Sonics & Materials Inc., USA). Following sonication, the nanoparticles (GaCeNPs) were centrifuged at 1500×*g* for 10 min and subsequently resuspended in deionised water. The relative amounts of lauryl gallate and ceragenin CSA-131 in the obtained GaCeNPs were estimated by quantifying the phenolic and amino content using Folin–Ciocalteu[18] and fluorescamine[19] assays, respectively. GaCeNPs were characterised by measuring their surface charge (ζ-potential) with a Zetasizer Nano Z (Malvern Instruments, Netherlands), particle size *via* transmission electron microscopy (TEM) using a JEOL JEM 2010F (JEOL Ltd, Japan), and antioxidant activity by the DPPH free radical scavenging method.[20] Antibacterial and antibiofilm properties were assessed by resazurin-based viability assay[21] and crystal violet staining,[22] respectively.

2.3 Surface functionalisation of silicone materials

Laminar pieces (1×1 cm, $n = 10$) of PDMS, used for production of urinary catheters, were washed sequentially with 0.1% (w/v) SDS solution, deionised water, and 96% ethanol. The pieces were then activated for 10 min with oxygen plasma in a reactor operating at 13.56 MHz frequency and 100 W power (Plasma System PE-25, Plasma Etch Inc., USA). Then, the samples were immersed in a 5% APTES (v/v) solution prepared in 96% ethanol and incubated for 24 h at room temperature. After washing with 96% ethanol to remove unbound APTES from the surface, the PDMS samples were incubated in 0.05 M acetate buffer solution (pH 5.0) containing 13.12 U mL^{-1} of laccase and 30% (v/v) of GaCeNPs. Subsequently, SB (0.5 M final concentration) was added to the solution and sonicated at 20 °C for 1 h with 50% ultrasound amplitude. Finally, the samples were rinsed with deionised water to eliminate the unbound reagents and dried under nitrogen gas flow. For the *in vitro* tests conducted in the hydrodynamic model of catheterised bladder, entire Foley catheters (size 16 French) were coated sono-enzymatically following the above described procedure.

2.4 Coating characterisation

Attenuated Total Reflectance-Fourier Transformed infrared (ATR-FTIR) spectra of both pristine and coated PDMS samples were recorded over the range of 650–4000 cm^{-1} using a PerkinElmer Spectrum 100 FTIR spectrometer (USA). Each spectrum was acquired by averaging 32 scans at a resolution of 4 cm^{-1}. The chemical composition of the coatings was characterised by X-ray photoelectron spectroscopy (XPS) using a SPECS Surface Nano Analysis system (SPECS Surface Nano Analysis GmbH), equipped with a high-intensity XR50 twin-anode X-ray source

(Mg/Al at 1253 eV/1487 eV) operating at 150 W. The X-ray source was aligned perpendicular to the analyser axis, and a Phoibos 150 MCD-9 XP detector was employed for signal collection. Survey and high-resolution spectra were acquired at pass energies of 25 eV and 0.1 eV, respectively. Charge compensation was achieved using a dual system of electron and argon ion flood guns, with electron energy/emission current set to 4 eV/0.35 mA and 0 eV/0.1 mA, respectively. Spectra were recorded in 0.1 eV steps at a pass energy of 25 eV under ultrahigh vacuum conditions (pressure $<6 \times 10^{-9}$ mbar). Standard charge neutralisation parameters were applied to ensure a uniform surface potential. The C 1s peak at 285.0 eV was used as an internal reference for binding energy calibration. The surface topography of both uncoated and coated samples was analysed by atomic force microscopy (AFM) (Dimension 3100 AFM system from Veeco, USA) operating in tapping mode, and the acquired images were processed using the Nanotec WSxM software (version Beta 9.2).[23] Water contact angles (WCA) of differently treated PDMS samples were measured using the sessile drop method with a Krüss DSA 25 (Germany) analyser. Data acquisition and analysis were performed with the Advanced v1.13.0.21301 software (Krüss), using the tangential method for WCA calculation. The stability of the coatings on the silicone materials was indirectly assessed by measuring the WCA of freshly treated PDMS samples and those incubated for 7 days (37 °C, 100 rpm) in ultrapure water.

2.5 Antibacterial, antifouling, and antibiofilm properties

2.5.1 Initial protein attachment. Silicone samples (1 × 1 cm) were incubated for 30 min in FITC-BSA solution (1 mg mL^{-1}) prepared in deionised water, to simulate the initial non-specific protein adsorption that precedes microbial colonisation and biofilm formation. Following incubation, the samples were rinsed with deionised water to remove unbound protein and subsequently dried with nitrogen. Protein adsorption on the pristine and coated silicones was assessed *via* fluorescence microscopy using a NIKON Eclipse Ti–S system (Nikon Instruments Inc., Japan).

2.5.2 Antibacterial activity. The antibacterial activity of the coated PDMS samples was evaluated following the ASTM-E2149-20 standard.[24] Individual colonies of *E. coli* and *S. aureus* were cultured overnight in 5 mL sterile MHB at 37 °C with agitation at 230 rpm. The bacterial cultures were then diluted in PBS (OD_{600} = 0.28). A further 1 : 1000 dilution was performed in PBS (0.1 M, pH 7.4), and each PDMS sample (1 × 1 cm) was incubated with 1.5 mL of the diluted bacterial suspension. After 24 h of incubation at 37 °C, the bacterial suspensions were collected, serially diluted, and plated onto selective agar media: Coliform agar for *E. coli* and Baird–Parker agar for *S. aureus*. Colony-forming units (CFUs) were counted to determine bacterial viability and evaluate the antibacterial efficacy of the coated PDMS surfaces.

2.5.3 Biofilm inhibition. Biofilm inhibition was evaluated by quantifying the total biomass of *E. coli* and *S. aureus* formed on the surface of PDMS. Silicone samples (1 × 1 cm) were placed in a 24-well microplate with 1.5 mL of bacterial suspension (OD_{600} = 0.01) prepared in TSB, and incubated at 37 °C for 24 h under static conditions to allow bacterial attachment and subsequent biofilm development. Afterwards, samples were gently rinsed three times with 2 mL of sterile PBS (0.1 M, pH 7.4) to remove non-adherent (planktonic) cells. The biofilms were then fixed at 60 °C for 2 h, and quantified using the crystal violet staining method, as previously described.[6]

2.5.4 Assessment of bacteria viability in biofilms. To assess the viability of *E. coli* and *S. aureus* cells within the biofilm, two complementary methods were employed: the XTT reduction assay and the Live/Dead fluorescence staining approach. For the XTT assay, PDMS pieces (1 × 1 cm) were placed in a 24-well microplate and inoculated with 1.5 mL of bacterial suspension (OD_{600} = 0.01) prepared in TSB. The plate was then incubated under static conditions at 37 °C for 24 h to allow biofilm formation. After incubation, each sample was mixed with 1 mL of freshly XTT reagent, prepared according to the supplier's instructions. The samples were then incubated for 2 h at 37 °C to allow enzymatic reduction of the tetrazolium salt by metabolically active cells, resulting in the formation of a coloured, water-soluble formazan product. The absorbance of the solution was measured at 492 and 690 nm using an Infinite M200 microplate reader (Tecan, Austria). Bacterial viability within the biofilm was assessed as previously described.[25]

For Live/Dead staining, biofilm-covered PDMS samples were gently rinsed with PBS to remove planktonic cells and stained using the Live/Dead BacLight™ bacterial viability kit, following the manufacturer's protocol. The biofilms were examined using fluorescence microscopy at 20× magnification. SYTO 9, a green-fluorescent dye that stains live cells, was visualised using excitation/emission wavelengths of 480/500 nm. Propidium iodide, a red-fluorescent probe that stains dead cells, was detected using excitation/emission wavelengths of 490/635 nm. This approach enables qualitative assessment of biofilm morphology and the spatial distribution of viable and non-viable cells on PDMS surfaces.

2.5.5 Assessment of coatings' durability. An *in vitro* model replicating the conditions of a catheterised human bladder was employed to evaluate both the coating stability and its efficacy in inhibiting biofilm formation under dynamic flow conditions.[26] Pristine and coated silicone Foley catheters were inserted into the *in vitro* model, and the retention balloon was inflated using 5 mL of sterile PBS (0.1 M, pH 7.4). The bladder reservoir was subsequently filled to the level of the catheter eye with sterile artificial urine (pH 6.8), prepared in accordance with UNE EN1616 (Sterile Urethral Catheters for Single Use) and supplemented with *E. coli* and *S. aureus* at OD_{600} = 0.01. The system was maintained at 37 °C for a period of 7 days under continuous perfusion with artificial urine at a flow rate of 1 mL min^{-1} to simulate physiological urinary output. Upon completion of the exposure period, catheters were retrieved and the extent of biofilm formation on both the catheter tip and balloon was assessed using the XTT approach, as described before.

2.6 *In vitro* assessment of coating biocompatibility

Fibroblasts (BJ-5ta) were pre-seeded at a density of 4.5×10^4 cells per well in a sterile 24-well tissue culture-treated polystyrene plate. For cytotoxicity evaluation, pristine and coated PDMS samples (1 × 1 cm) were placed in direct contact with the cells for 1 and 7 days. Subsequently, 0.75 mL of DMEM was added to each well, and the plate was incubated at 37 °C in a humidified atmosphere with 5% CO_2 for 24 h. Cell viability was assessed using the AlamarBlue assay kit, following the manufacturer's instructions. Cells cultured under the same conditions without PDMS samples served as negative controls. Fibroblast viability was also evaluated using the Live/Dead® Viability/Cytotoxicity kit, according to the supplier's protocol. Fluorescence microscopy was employed to visualise viable and non-viable cells, providing qualitative confirmation of biocompatibility.

2.7 Statistical analysis

Data were presented as the mean ± standard deviation (S.D.). Statistical analysis was performed using the GraphPad Prism Software (version 5.04). For comparisons between two groups, an unpaired two-tailed Student's *t*-test was used. For comparisons involving more than two groups, one-way analysis of variance (ANOVA) followed by a post-hoc Tukey's test was applied. Statistical significance was considered at p-values <0.05 (*), < 0.01 (**), or < 0.001 (***), indicating different levels of significance.

3. Results and discussion

3.1 Synthesis and characterisation of GaCeNPs

The ultrasound-assisted emulsification method used in this work for the synthesis of GaCeNPs proved to be a straightforward strategy for producing nanostructures stabilised through multiple non-covalent interactions occurring primarily at the shell, including hydrogen bonding between the phenolic moieties of lauryl gallate and amino groups of CSA-131, cation-π, and π–π stacking between the aromatic rings (Fig. 1A). Moreover, GaCeNPs exhibited a homogeneous size distribution (∼200 nm), as confirmed by TEM imaging (Fig. 1B). Both lauryl gallate nanoparticles (GaNPs) and GaCeNPs showed good colloidal stability, as indicated by ζ-potential values of −35 ± 1 mV and +25 mV, respectively. The shift from negative to positive ζ-potential is attributed to the presence of CSA-131, a synthetic amphipathic molecule, and the surface orientation of its amino group-bearing hydrophilic head on the GaCeNP. Quantification of phenolic and amino groups revealed a lauryl gallate to ceragenin (CSA-131) molar ratio of approximately 4 : 1 in the obtained nanostructures. Altogether, these findings suggest that both lauryl gallate and CSA-131 are localised at the nanoparticle shell, where their respective groups contribute to the structural stability and functionalities of GaCeNPs.

The high content of lauryl gallate also contributes to the antioxidant properties of GaCeNPs (Fig. S1). Additionally, GaNPs and GaCeNPs inhibited the growth (Fig. 2A) and biofilm formation (Fig. 2B) of *S. aureus* and *E. coli*. A synergistic antibacterial effect was observed for GaCeNPs, where the combination of lauryl gallate and the antimicrobial ceragenin enhanced both antibacterial and antibiofilm activities. Lauryl gallate inserts into bacterial membranes due to its amphiphilic nature, disturbing the lipid bilayer. This disruption compromises membrane integrity, leading to leakage of cellular contents and impaired bacterial viability. Alkyl gallates have been also reported to antagonise quorum sensing receptors, thus interfering with the signalling pathways that bacteria use to regulate virulence and biofilm formation.[13,27] In addition, CSA-131, a synthetic small molecule designed to mimic the

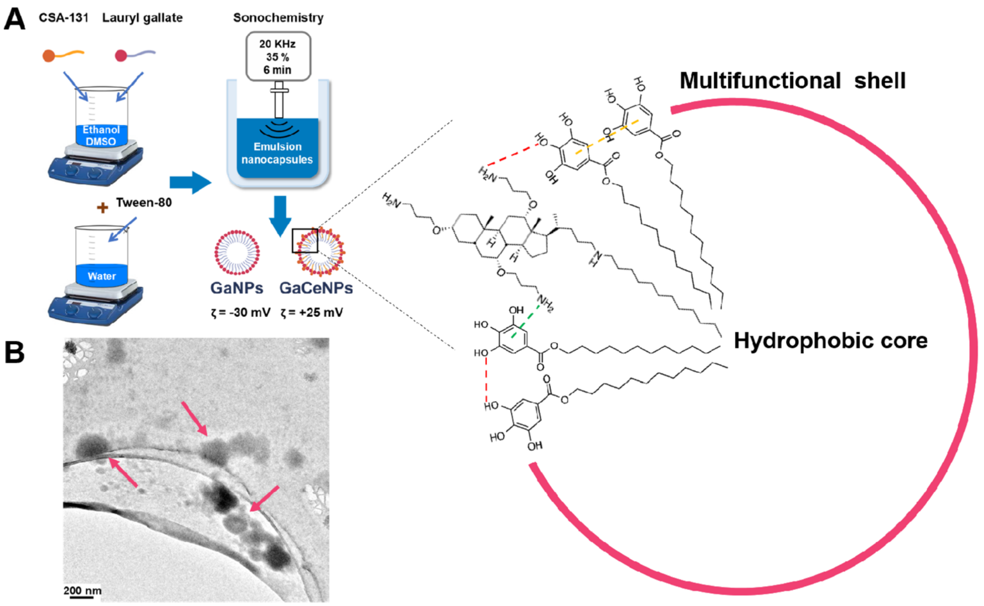

Fig. 1 (A) Schematic representation of GaCeNPs synthesis and assembly, where the red dashed line represents the hydrogen bonding, the yellow dashed line indicates π–π stacking between lauryl gallate and CSA-131 and green dashed line represent cation-π interaction. (B) A representative TEM image of the obtained GaCeNPs. The pink arrows indicate distinct spherical GaCeNPs deposited onto the TEM grid.

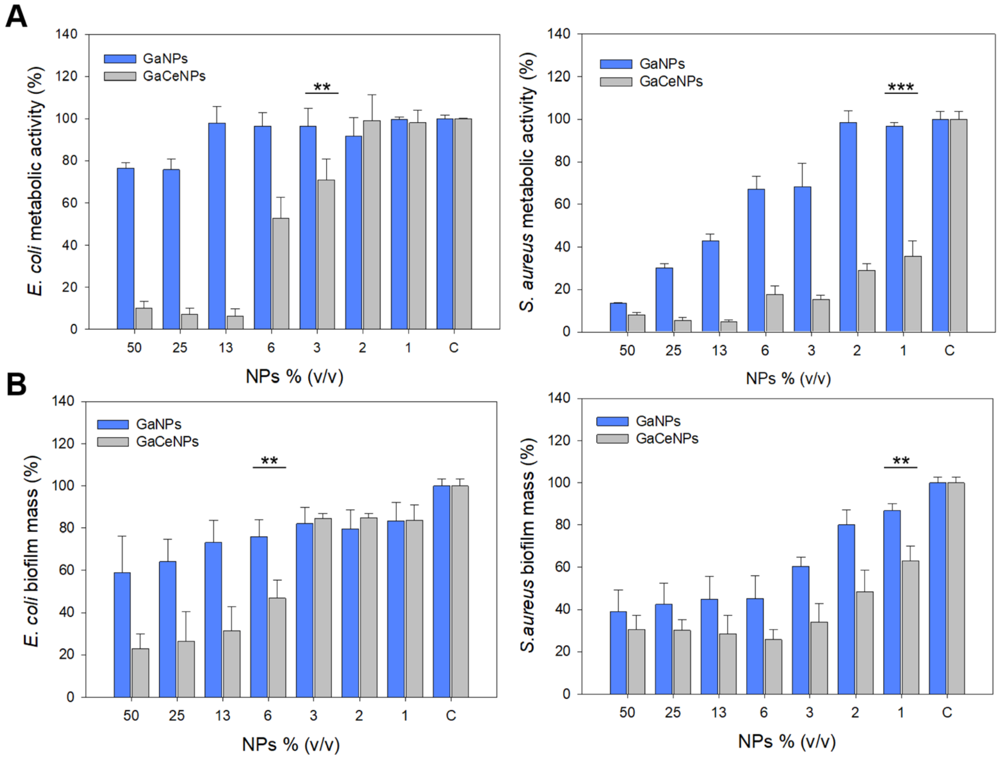

Fig. 2 (A) Antibacterial activity of GaCeNPs evaluated by resazurin-based viability assay, and (B) biofilm inhibition assessed by crystal violet staining against *E. coli* and *S. aureus*. Data are presented as the mean value ± S.D. ($n = 3$).

function of cationic antimicrobial peptides, induces membrane depolarisation and permeabilisation.[15,28] The inclusion of ceragenin in GaCeNPs significantly improved their antibacterial performance at lower concentrations compared to GaNPs alone, against both Gram-positive and -negative bacteria.

3.2 Physicochemical characterisation of the nanocomposite coatings

Following the pre-activation and amination of the silicone substrate, the functional coating was generated through a single-step ultrasound-potentiated synthetic process,

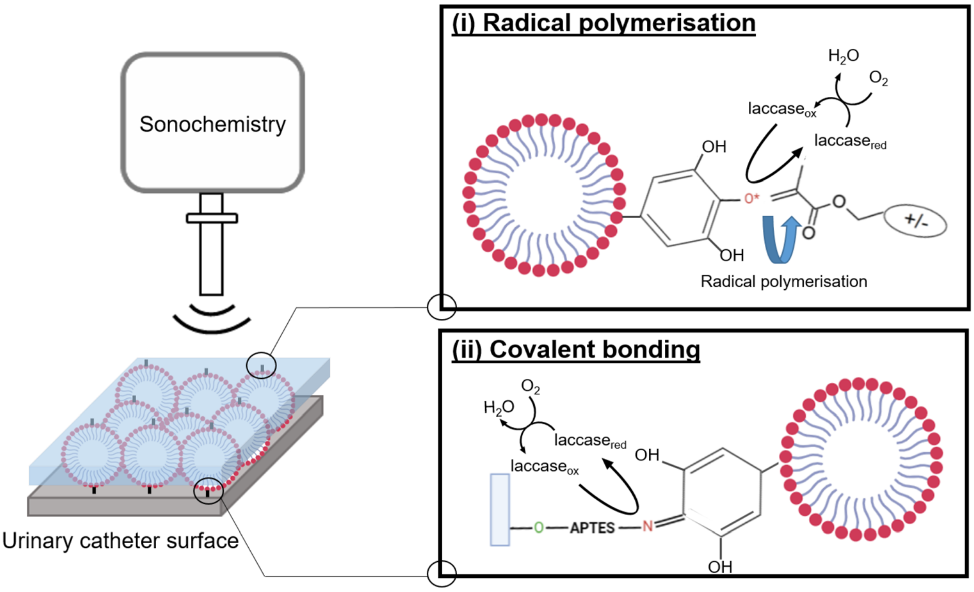

Fig. 3 Schematic representation of the bottom-up strategy for nano-enabled coating synthesis, illustrating the sono-enzymatic grafting of GaCeNPs and polymerisation of SB.

integrating two concurrent reactions: (i) laccase-catalysed grafting of GaCeNPs onto the aminated silicone surface *via* oxidative coupling of phenolic moieties, and (ii) radical polymerisation of SB leading to the formation of a pSB layer (Fig. 3 and S2).

After pre-activation of the silicone samples with oxygen plasma, APTES was chemisorbed to provide primary amino groups, which may act as reactive sites (nucleophilic anchors) on the otherwise inert silicone surface. This initial modification was confirmed by the appearance of two distinctive peaks in the FTIR-ATR spectrum of the pre-treated PDMS at 1485 and 1575 cm^{-1} (Fig. 4A), together with the appearance of a new signal at 400 eV in the respective N 1s (Fig. 4B), which can be assigned to CH$_2$ bending vibrations of the APTES alkyl chain and N–H bending (scissoring) modes of the NH$_2$ groups, respectively.[2,29] The successful immobilisation of GaCeNPs on the APTES-aminated silicone surface was evidenced by the disappearance of the bands at 1485 cm^{-1} and 1575 cm^{-1}, associated with phenolic groups, and the appearance of a new shoulder at 1650 cm^{-1}. This new band can be attributed to overlapping vibrations of quinone carbonyl (C=O) stretching and imine (C=N) functionalities. Additionally, the analysis of C 1s XPS spectrum after grafting GaCeNPs revealed the presence of new C–O–C/C–OH (287–289 eV) from the different functional groups in the GaCeNPs (Fig. 4C). These spectral changes are consistent with the laccase-catalysed oxidation of phenolic groups in the gallate moieties, generating highly reactive *o*-quinones. These quinones subsequently react with nucleophilic amino groups on the surface yielding imine bonds through Schiff base formation, and form additional covalent bonds *via* Michael-type addition reactions.[8] Additionally, a distinct peak was observed at 1721 cm^{-1}, attributed to the C=O stretching vibration of the ester group in lauryl gallate, further confirming the presence of GaCeNPs on the coated surface. In addition to surface anchoring, the reactive *o*-quinones generated from lauryl gallate can also react with primary amines from the GaCeNPs, resulting in intra- and inter-particle crosslinking that further stabilises the nanocomposite. This cross-linking process is evidenced by the observed reduction in both free phenolic and primary amine functionalities in the GaCeNPs

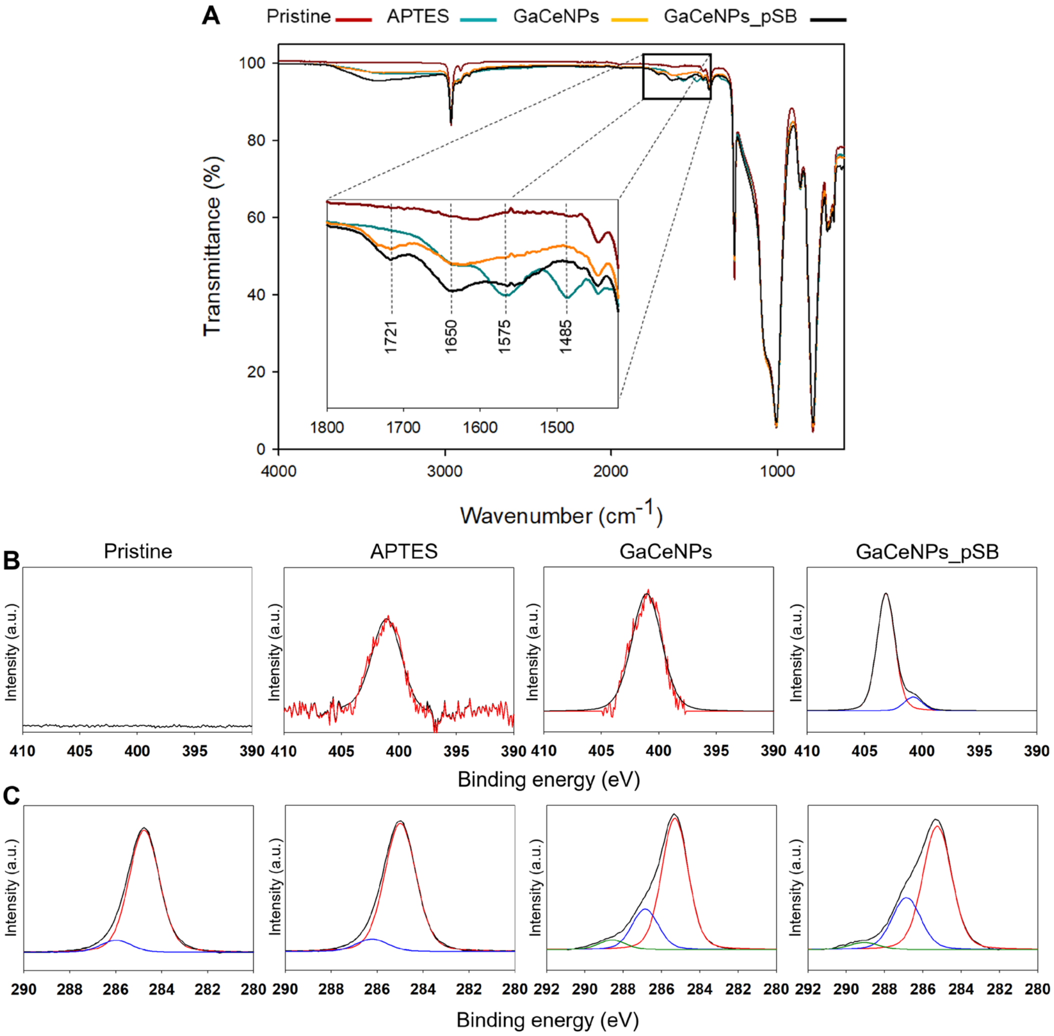

Fig. 4 (A) FTIR-ATR spectra of pristine PDMS and samples corresponding to successive surface modification steps during the coating process. (B) High-resolution XPS spectra of N 1s, (C) high-resolution XPS spectra of C 1s.

after exposure to the same reaction conditions employed during the coating formation (Fig. S3).

The coating formation (Fig. 3) involved the surface-initiated radical polymerisation of SB monomers, triggered by phenoxy radicals enzymatically generated from gallate groups that had not reacted during GaCeNPs grafting or subsequent crosslinking. The successful formation of the pSB layer was confirmed by the appearance of a new peak in the N 1s XPS spectra, attributed to the quaternary ammonium group. Additionally, the presence of the polyzwitterionic layer was further supported by the appearance of an intensified broad shoulder around 3500 cm^{-1} in the FTIR spectra, attributed to –OH stretching vibrations consistent with the presence of hydrophilic polymer chains. This spectral feature is characteristic of the polymerised zwitterionic coating. Notably, the peaks at 1650 cm^{-1} and 1721 cm^{-1}, associated with GaCeNPs, also showed increased intensity in the GaCeNPs_pSB-coated silicone. This may result from the presence of SB in the reaction medium during the sonochemical coating process. SB is known to stabilise enzymes,[30] which could enhance laccase-assisted oxidation, further facilitating more efficient functionalisation of GaCeNPs onto the silicone surface. Despite the moderate colloidal stability of GaCeNPs (ζ-potential ≈ +25 mV) the zwitterionic nature of SB also provides steric hindrance and electrostatic repulsion that may further contribute to suppressing nanoparticle aggregation and promoting a more effective attachment of the GaCeNPs_pSB coating on silicone.

In terms of surface morphology, AFM analysis showed that pristine silicone exhibited a relatively smooth surface (Fig. 5A), with a root mean square roughness (R_q) of 44.6 nm (Fig. 5B). Upon silanisation with APTES, the surface roughness decreased (R_q = ∼11 nm), likely due to the formation of an uniform aminated layer on the treated PDMS samples. Following the enzymatic immobilisation of GaCeNPs, the silicone surface exhibited increased heterogeneity and the R_q increased to 87.1 nm (Fig. 5B) due to the nanoparticle deposition and the formation of some surface irregularities, visible in Fig. 5A. This may be explained by the high reactivity of the oxidised phenolic groups in the gallate moieties, which lead to dual-level nanoparticle crosslinking as previously mentioned. Interestingly, as the reaction progressed, the *in situ* polymerisation of the zwitterionic SB monomer led to smoother surface, as evidenced by roughness reduction (R_q ∼60 nm; Fig. 5B). Although discrete surface nodes were observed (Fig. 5A), the R_q value was lower

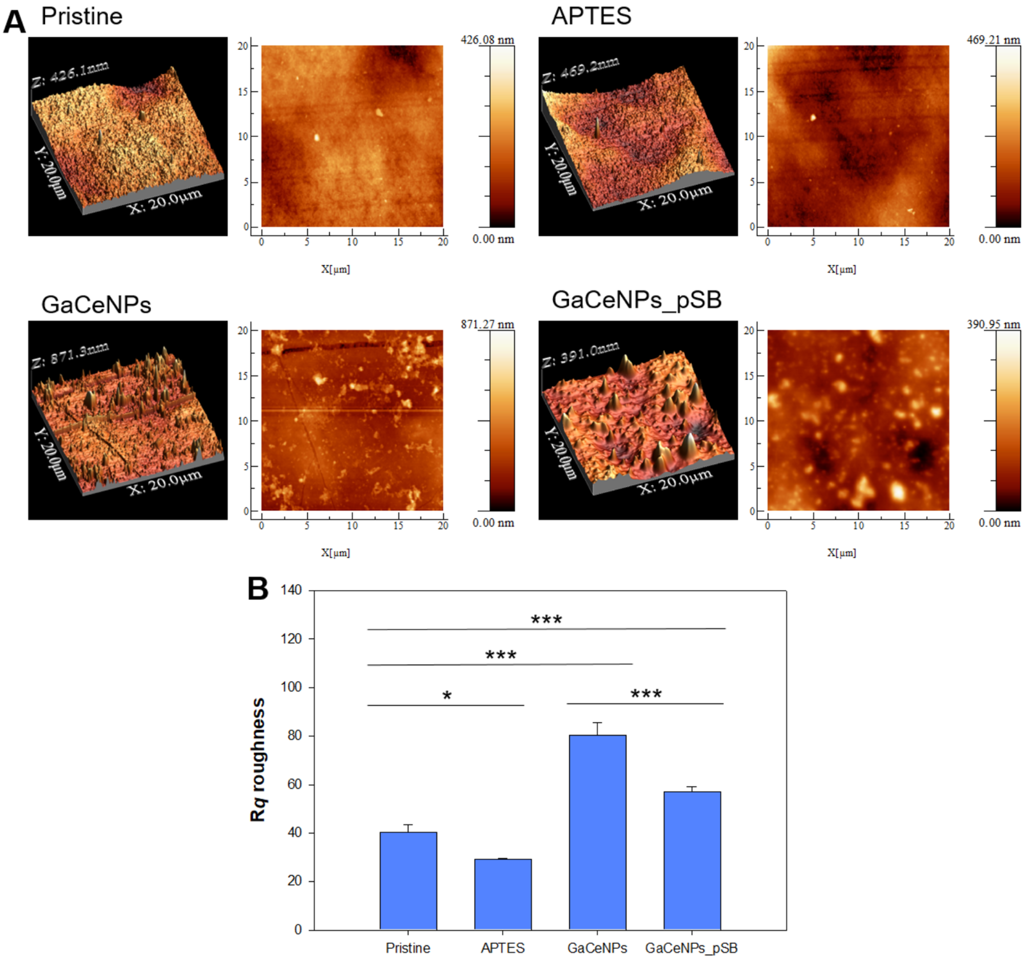

Fig. 5 (A) Representative AFM-derived 3D surface morphologies and (B) corresponding root mean square roughness (R_q) values of pristine and modified PDMS surfaces at each step of the coating process. Data are presented as the mean value ± S.D. (n = 3).

than that of the GaCeNPs-coated silicone. This reveals that the GaCeNPs_pSB-coated surface is morphologically more uniform, effectively minimising the nanoscale surface height variations despite the presence of localised features. This smoother surface morphology, together with the intrinsic hydrophilicity of zwitterionic polymers, suggests the formation of a homogeneous hydrogel-like coating.[31] Consequently, the GaCeNPs_pSB coating could reduce the mechanical friction or abrasion against tissue during catheter insertion and removal, thereby minimising trauma and improving biocompatibility.

While the impact of surface roughness on bacterial adhesion remains under debate, intermediate roughness levels have been associated with increased microbial retention, whereas very smooth (providing fewer attachment points) or highly irregular surfaces (which roughness scale larger than the bacteria), tend to be less susceptible to bacterial contamination.[32] GaCeNPs_pSB-coated silicone exhibited an R_q value of approximately 60 nm (within the intermediate range) yet its zwitterionic and lauryl gallate–ceragenin CSA-131 composition may counteract microbial retention through both antifouling and antibacterial activity. Furthermore, this level of surface roughness is comparable to that of commercial urinary catheters and, when combined with the hydrophilic and presumably hydrogel-like character of the GaCeNPs_pSB coating, is not expected to compromise lubricity or patient comfort.[33]

3.3 Surface wettability, stability, and antifouling properties of functionalised silicone

To evaluate the wettability and indirectly assess the surface stability of the developed coating, WCA measurements were performed after one week of incubation in water (Fig. 6A). The contact angle decreased progressively during the functionalisation stages (Fig. 3), indicating an increase in surface hydrophilicity throughout the coating process. As expected, APTES functionalisation reduced the surface hydrophobicity of the PDMS samples due to the incorporation of hydrophilic amine groups. The unmodified silicone initially displayed a water contact angle of around 114°, indicative of its intrinsic hydrophobic character. Upon grafting with GaCeNPs, the contact angle further decreased by approximately 20° compared to the pristine material and ∼10° from the aminated surface, reflecting a progressive increase in surface wettability. This effect is attributable to the phenolic groups of lauryl gallate, which is the predominant component in the GaCeNPs, as previously described. The higher proportion of gallate-derived hydroxyl groups contributes to the enhanced hydrophilicity observed. Subsequent polymerisation of the zwitterionic SB monomer further increased the surface hydrophilicity. This is consistent with the high water absorption and strong hydration capacity reported for pSB-based coatings.[34] Notably, the WCA values remained unchanged after 7 days of incubation in water, indicating that the coating functionalisation of the silicones remain stable (Fig. 6A).

Given the biological relevance of protein interactions with catheters, further measurements were conducted to assess the antifouling performance of the coatings. An increased presence of plasma proteins in urine is commonly observed in patients with urinary tract infections, often reflecting inflammation or epithelial disruption. Proteins can adsorb non-specifically onto hydrophobic materials such as silicone, potentially providing a conditioning layer that facilitates bacterial adhesion and supports subsequent biofilm development.[35] Increasing the hydrophilicity of the catheter surface can mitigate this effect by forming a stable hydration layer, which creates an energetically-unfavourable interface for the adsorption of hydrophobic proteins.[36] As seen in Fig. 6B, silicone samples coated with GaCeNPs and GaCeNPs_pSB effectively prevented the non-specific adsorption of FITC-labelled BSA, with slightly improved performance observed for GaCeNPs_pSB. This observation supports the antifouling behaviour of zwitterionic coatings, attributed to the formation of a tightly bound hydration layer that effectively prevents protein attachment.[37]

3.4 Antibacterial and antibiofilm properties of the nanocomposite coatings

The GaCeNPs- and GaCeNPs_pSB-coated silicone exhibited potent antibacterial activity against *E. coli* and *S. aureus*, two of

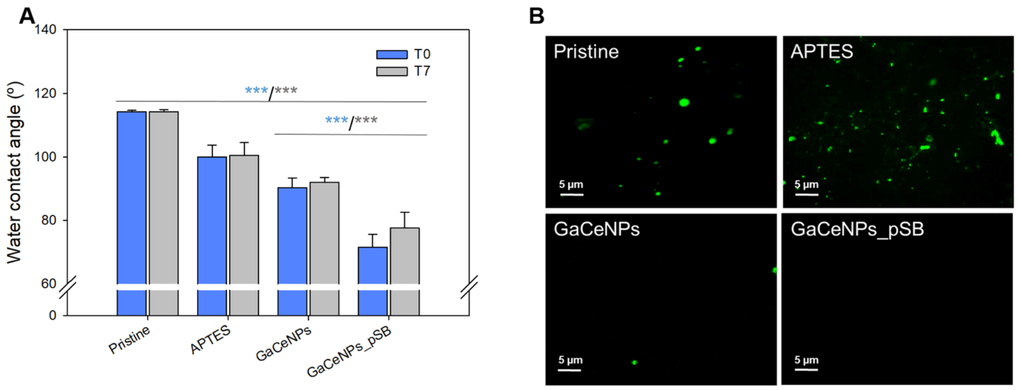

Fig. 6 (A) Water contact angle of pristine and treated silicone samples. The blue bars represent the values obtained immediately after the functionalisation or coating deposition, while the grey bars represent the values obtained after 7-day incubation in ultrapure water (at 37 °C, with 100 rpm agitation). Data are presented as the mean value ± S.D. ($n = 3$). (B) Fluorescence images of pristine and treated silicone samples taken after 30 min of incubation in a 1 mg per mL solution of FITC-labelled BSA. Scale bar: 5 µm.

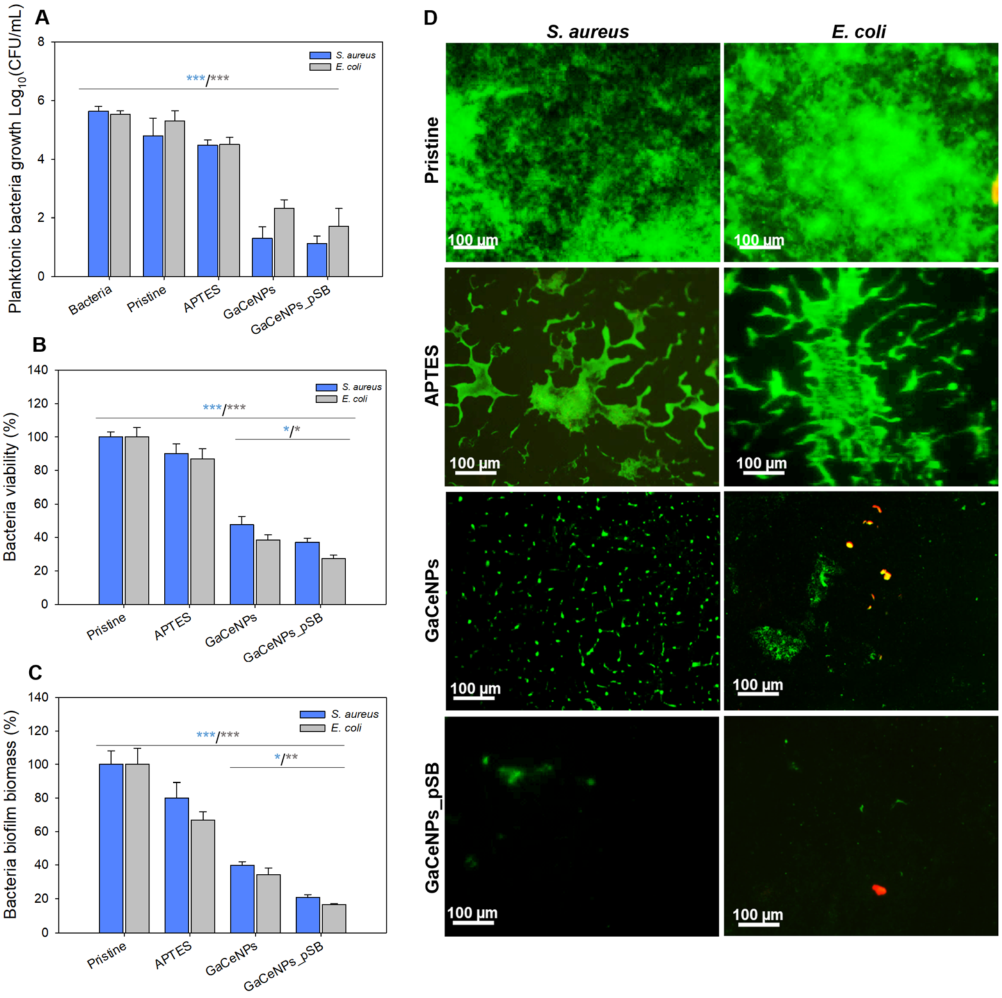

Fig. 7 (A) Quantification of planktonic bacteria after 24 h exposure of pristine and functionalised silicone samples to *S. aureus* or *E. coli* suspensions. (B) Viability of *S. aureus* and *E. coli* cells within biofilms, and (C) total biomass formation on control (pristine) and functionalised silicone surfaces under static conditions. Data are presented as the mean value ± S.D. ($n = 3$). (D) Fluorescence microscopy images of live (green) and dead (red) cells in biofilms on pristine and functionalised PDMS pieces. Green and red fluorescence images are overlapped. Scale bar: 100 μm.

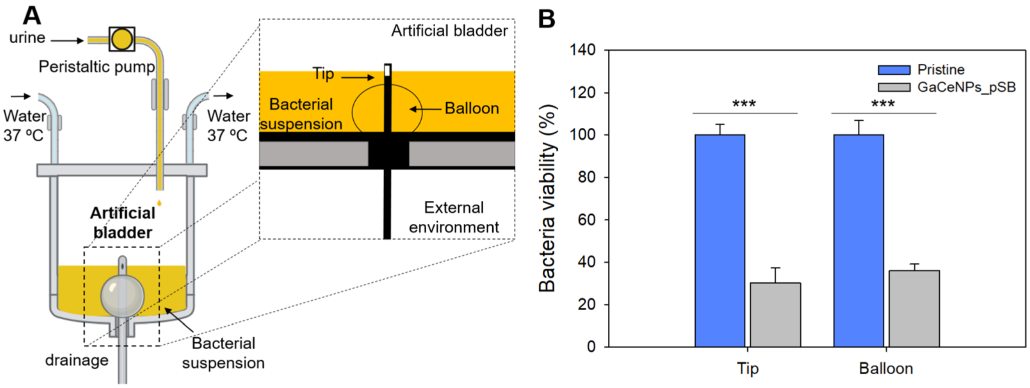

Fig. 8 (A) Schematic representation of the experimental setup simulating a human bladder. (B) Biofilm biomass quantification on pristine and GaCeNPs_pSB-coated catheter sections (tip and balloon) following 7 days of incubation with recirculating infected urine in the artificial bladder system. Data are presented as the mean value ± S.D. ($n = 3$).

the most common pathogens implicated in biofilm formation on catheters (Fig. 7A). After 24 h of incubation, the presence of GaCeNPs in the coatings led to an approximately 3-log reduction in planktonic bacterial counts compared to pristine silicone, confirming the antibacterial efficacy of the nano-enabled surfaces against both microorganisms. Although the pSB layer did not enhance the antibacterial activity of the coated silicones against free-floating bacteria, it significantly improved its antibiofilm performance. Both bacterial viability (Fig. 7B) and biofilm mass accumulation (Fig. 7C) on GaCeNPs_pSB-coated silicone were reduced by 70–80%, likely due to the synergistic action of the bioactive GaCeNPs (Fig. 2) and the antifouling properties of the zwitterionic polymer (Fig. 6A). Furthermore, biofilm biomass and bacterial viability within the biofilms were qualitatively evaluated using Live/Dead fluorescence staining (Fig. 7D). Pristine and APTES-modified surfaces exhibited dense biofilm coverage of viable bacteria, as indicated by strong green fluorescence. In contrast, GaCeNPs-coated silicone showed a substantial reduction in biofilm formation and viability, evidenced by the presence of yellow- and red-stained cells, consistent with a contact-killing mechanism. However, viable cells remained adhered to the surface, indicating incomplete biofilm suppression. Notably, GaCeNPs_pSB-coated samples demonstrated greater inhibition of biofilm formation, with significantly lower fluorescence observed. These results underscore the synergistic effect of the zwitterionic layer, which imparts antifouling protection that complements the antibacterial activity of the embedded GaCeNPs.

Additionally, the antibiofilm efficacy of the GaCeNPs_pSB coating was evaluated using an experimental setup that simulates a human bladder (Fig. 8A). Pristine and coated Foley catheters were inserted into the model bladder inoculated with a mixed suspension of *S. aureus* and *E. coli* prepared in artificial urine. The system was perfused at a flow rate of 1 mL min^{-1}, selected to replicate the flow through urinary catheters connected to drainage bags, and to achieve a daily urine output equivalent to that of an adult (0.8–2.0 L).[38] After 7 days of infected urine recirculation, the catheters were retrieved, segmented, and analysed to quantify the amount of bacterial biofilm formed on two specific catheter areas: the tip with the

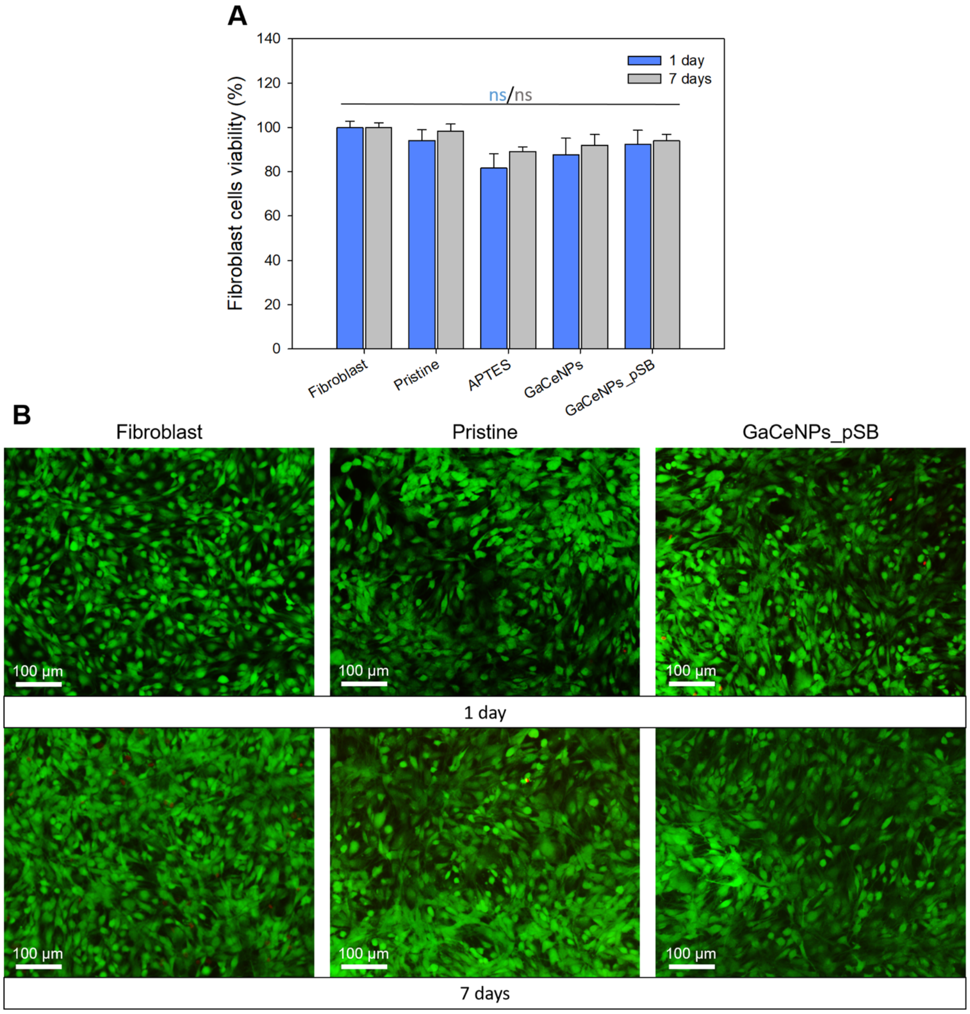

Fig. 9 Fibroblast (BJ-5ta) viability after 24 h and 7 days in direct contact with pristine and functionalised silicone samples, assessed by (A) AlamarBlue assay and (B) Live/Dead staining. Data are presented as the mean value ± S.D. ($n = 3$). Green and red fluorescence images are overlaid.

drainage hole that allows urine to flow through the catheter tubing, and the balloon. A 70% reduction in the viability of surface-attached bacteria was observed for GaCeNPs_pSB-coated catheters compared to the pristine control (Fig. 8B), demonstrating durable antibacterial activity even after 7 days under simulated conditions closely mimicking real-life application.

3.5 Cytotoxicity evaluation

Biocompatibility is a critical prerequisite in the development of medical devices that interface with human tissues. Therefore, any device coating must preserve the inherent cytocompatibility of the underlying material. The broad-spectrum and strong bactericidal activity of CSA-131 at low concentrations through non-specific membrane-disruptive mechanisms,[39] may raise concerns about potential cytotoxicity on human cells when incorporated in the catheter coating. To evaluate this, fibroblast viability was assessed after 24 h and 7 days of direct contact with the coated silicone samples. All modified specimens maintained fibroblast viability above 90%, with no statistically significant differences compared to pristine silicone (Fig. 9A). This is particularly important given that fibroblasts are major stromal cells in the urogenital tract and play a critical role in tissue structure and repair.

Fluorescence microscopy (Fig. 9B) further corroborated the viability data, showing that the cells retained their characteristic elongated morphology and confluence at both tested time points. Therefore, GaCeNPs and GaCeNP_pSB coatings, despite incorporating a potent bactericidal agent (*i.e.*, CSA-131), did not compromise fibroblast viability or morphology even after 7 days of contact. This timeframe is clinically-relevant, as some protocols recommend catheter replacement within 7 days to minimise the risk of catheter-associated complications. Such results support the cytocompatibility of the coated catheters for potential clinical application. Moreover, these findings imply that the coatings do not leach toxic substances at levels harmful to human cells, indicating a favourable safety profile under the tested conditions. Notably, this represents a clear advantage over metal-based nanoparticle coatings, which often pose cytotoxicity risks due to uncontrolled metal ion release.[9]

4. Conclusions

A multifunctional coating for urinary catheters was synthesised *via* a bottom-up sono-enzymatic approach, in which laccase-mediated oxidation enabled the covalent grafting of GaCeNPs, obtained through ultrasonic emulsification, onto the aminated silicone substrate. Oxidised phenolic groups on the GaCeNPs-grafted surface consequently initiated the radical polymerisation of sulfobetaine vinyl monomers, resulting in a hydrophilic pSB layer with antifouling properties and moderate surface roughness. The resulting nanocomposite coating prevented non-specific protein attachment and remained stable after a week of incubation in water, maintaining its surface hydrophilicity. In addition, the viability of planktonic *E. coli* and *S. aureus* were significantly reduced upon contact with the GaCeNPs_pSB-coated silicone, while also inhibiting early biofilm formation on its surface. Both antibacterial and antibiofilm effects were attributed to the synergistic action of the antimicrobial CSA-131 and the antifouling zwitterionic polymer. The antimicrobial efficacy of GaCeNPs_pSB-coated Foley catheters was further validated using a hydrodynamic model that replicates the catheterised bladder under physiological flow, demonstrating sustained antibiofilm activity over a clinically relevant 7-day period. Importantly, GaCeNPs_pSBs-coated silicone showed no adverse effects on major stromal cell types found in the urogenital tract. These findings not only confirm the biosafety of the developed coating but also support the transition towards fully organic, antibiotic- and metal-free coatings for biomedical devices, addressing antibacterial resistance and cytotoxicity issues. Overall, this study highlights the potential of laccase-mediated surface functionalisation, supported by ultrasound-assisted deposition, to enable durable, antibacterial, and anti-fouling biopolymer coatings on urinary catheters.

Author contributions

A. P.-S., and T. T. conceived the idea and planned the experiments. A. P.-S., and K. I. prepared and characterised the NPs. A. P.-S., L. M. P. and P. S., carried out antibacterial, antibiofilm test and cytotoxicity studies. A. P.-S., G. C., L. M. P., P. S., and T. T. data analysed and validation. A. P.-S., K. I., L. M. P., wrote the manuscript. P. S., G. C., and T. T. manuscript review and editing. K. I. and T. T. acquired funding and supervised the study.

Conflicts of interest

The authors declare that they have no competing interests.

Data availability

The data supporting this article have been included as part of the SI.

Supporting information includes data on the antioxidant activity of GaCeNPs, a schematic representation of the coating production process, and the enzymatic autografting of the nanoparticles following the laccase-mediated reaction. See DOI: **https://doi.org/10.1039/d5na00577a**.

Acknowledgements

The authors acknowledge the grant PCI2024-153444 (SMART-GEL – Smart nanogels of bio-based antimicrobials to prevent urinary tract infections by disrupting inter- and intra-species communication of pathogens), funded by Agencia Estatal de Investigación (Ministerio de Ciencia e Innovación, España), under the European Union M-ERA.NET initiative. T. T. acknowledges the ICREA Academia award.

References

1 M. J. Andersen and A. L. Flores-Mireles, *Coatings*, 2020, **10**, 1–25.

2 A. Puertas-segura, A. G. Morena, P. Silvia, K. Ivanova, I. Ivanov, K. Todorova, P. Dimitrov, G. Ciardelli and T. Tzanov, *ACS Appl. Mater. Interfaces*, 2024, **16**, 39129–39139.

3 N. Sabir, A. Ikram, G. Zaman, L. Satti, A. Gardezi, A. Ahmed and P. Ahmed, *Am. J. Infect. Control*, 2017, **45**, 1101–1105.

4 F. Bull, S. Tavaddod, N. Bommer, M. Perry, C. A. Brackley and R. J. Allen, *Nat. Commun.*, 2025, **16**, 3940.

5 M. Ramstedt and M. Burmølle, *Curr. Opin. Biomed. Eng.*, 2022, **22**, 100370.

6 A. Puertas-Segura, K. Ivanova, L. M. Pérez, B. E. O. Z. El Abidine, A. Ivanova, B. Gökalsın, G. Ciardelli and T. Tzanov, *Adv. Mater. Interfaces*, 2025, **12**, 2401016.

7 S. Dai, Y. Gao and L. Duan, *J. Appl. Polym. Sci.*, 2023, **140**, 1–15.

8 C. Diaz Blanco, A. Ortner, R. Dimitrov, A. Navarro, E. Mendoza and T. Tzanov, *ACS Appl. Mater. Interfaces*, 2014, **6**, 11385–11393.

9 E. Janik-Karpinska, R. Brancaleoni, M. Niemcewicz, W. Wojtas, M. Foco, M. Podogrocki and M. Bijak, *Healthc*, 2023, **11**, 1–14.

10 X. Lai, Y. Feng, J. Pollard, J. N. Chin, M. J. Rybak, R. Bucki, R. F. Epand, R. M. Epand and P. B. Savage, *Acc. Chem. Res.*, 2008, **41**, 1233–1240.

11 A. Puertas-Segura, A. Laganá, G. Rathee, P. Savage, K. Todorova, P. Dimitrov, I. Pashkuleva, R. L. Reis, G. Ciardelli and T. Tzanov, *ACS Appl. Mater. Interfaces*, 2025, DOI: **10.1021/acsami.5c13979**.

12 I. Kubo, N. Masuoka, P. Xiao and H. Haraguchi, *J. Agric. Food Chem.*, 2002, **50**, 3533–3539.

13 M. Rayan, S. A. Lafi, M. Falah, T. Kacergius, A. Kirkliauskiene, V. Gabe and A. Rayan, *Molecules*, 2023, **28**, 1751.

14 U. Wnorowska, E. Piktel, P. Deptuła, T. Wollny, G. Król, K. Głuszek, B. Durnaś, K. Pogoda, P. B. Savage and R. Bucki, *Sci. Rep.*, 2022, **12**, 1–16.

15 M. Karasiński, U. Wnorowska, B. Durnaś, G. Król, T. Daniluk, K. Skłodowski, K. Głuszek, E. Piktel, S. Okła and R. Bucki, *Pathogens*, 2023, **12**, 1346.

16 H. Pelling, J. Nzakizwanayo, S. Milo, E. L. Denham, W. M. MacFarlane, L. J. Bock, J. M. Sutton and B. V. Jones, *Lett. Appl. Microbiol.*, 2019, **68**, 277–293.

17 C. Li, A. S. Peters, E. L. Meredith, G. W. Allman and P. B. Savage, *J. Am. Chem. Soc.*, 1998, **120**, 2961–2962.

18 R. O. Vernon, L. Singleton and R. M. Lamuela-Raventós, *Lipids*, 1968, **3**, 561.

19 S. Udenfriend, S. Stein, P. Böhlen, W. Dairman, W. Leimgruber and M. Weigele, *Science*, 1972, **178**, 871–872.

20 W. Brand-Williams, M. E. Cuvelier and C. Berset, *LWT–Food Sci. Technol.*, 1995, **28**, 25–30.

21 J. L. Chen, T. W. J. Steele and D. C. Stuckey, *Biotechnol. Bioeng.*, 2018, **115**, 351–358.

22 K. Ivanova, A. Ivanova, J. Hoyo, S. Pérez-Rafael and T. Tzanov, *Int. J. Mol. Sci.*, 2022, **23**, 7632.

23 I. Horcas, R. Fernández, J. M. Gómez-Rodríguez, J. Colchero, J. Gómez-Herrero and A. M. Baro, *Rev. Sci. Instrum.*, 2007, **78**, 013705.

24 ASTM International, Standard test method for determining the antimicrobial activity of immobilized antimicrobial agents under dynamic conditions, *Annual Book of ASTM Standards*, 2020.

25 J. Blair, G. Rathee, A. Puertas-Segura, L. M. Pérez and T. Tzanov, *Environ. Res.*, 2025, **279**, 121783.

26 A. Puertas-segura, K. Ivanova, A. Ivanova, I. Ivanov, K. Todorova, P. Dimitrov, G. Ciardelli and T. Tzanov, *ACS Appl. Mater. Interfaces*, 2024, **16**, 34656–34668.

27 B. Kim, J. S. ParK, H. Y. Choi, J. H. Kwak and W. G. Kim, *Sci. Rep.*, 2019, **9**, 1–12.

28 M. M. Hashemi, B. S. Holden, M. F. Taylor, J. Wilson, J. Coburn, B. Hilton, T. Nance, S. Gubler, C. Genberg, S. Deng and P. B. Savage, *Molecules*, 2018, **23**, 596.

29 N. Majoul, S. Aouida and B. Bessaïs, *Appl. Surf. Sci.*, 2015, **331**, 388–391.

30 R. Rajan and K. Matsumura, *Polym. Chem.*, 2024, **15**, 2040–2046.

31 M. Yao, Z. Wei, J. Li, Z. Guo, Z. Yan, X. Sun, Q. Yu, X. Wu, C. Yu, F. Yao, S. Feng, H. Zhang and J. Li, *Nat. Commun.*, 2022, **13**, 5339.

32 M. Mu, S. Liu, W. DeFlorio, L. Hao, X. Wang, K. S. Salazar, M. Taylor, A. Castillo, L. Cisneros-Zevallos, J. K. Oh, Y. Min and M. Akbulut, *Langmuir*, 2023, **39**, 5426–5439.

33 D. S. Jones, C. P. Garvin and S. P. Gorman, *Biomaterials*, 2004, **25**, 1421–1428.

34 Q. Li, C. Wen, J. Yang, X. Zhou, Y. Zhu, J. Zheng, G. Cheng, J. Bai, T. Xu, J. Ji, S. Jiang, L. Zhang and P. Zhang, *Chem. Rev.*, 2022, **122**, 17073–17154.

35 T. Mohan, A. Čas, M. Bračič, O. Plohl, A. Vesel, M. Rupnik, L. F. Zemljič and J. Rebol, *ACS Biomater. Sci. Eng.*, 2019, **5**, 5825–5832.

36 M. He, K. Gao, L. Zhou, Z. Jiao, M. Wu, J. Cao, X. You, Z. Cai, Y. Su and Z. Jiang, *Acta Biomater.*, 2016, **40**, 142–152.

37 X. Han, C. Leng, Q. Shao, S. Jiang and Z. Chen, *Langmuir*, 2019, **35**, 1327–1334.

38 E. P. Van Haarst, E. A. Heldeweg, D. W. Newling and T. J. Schlatmann, *BJU Int.*, 2004, **93**, 1257–1261.

39 M. Karasiński, U. Wnorowska, T. Daniluk, P. Deptuła, M. Łuckiewicz, P. Paprocka, B. Durnaś, K. Skłodowski, B. Sawczuk, P. B. Savage, E. Piktel and R. Bucki, *Int. J. Mol. Sci.*, 2024, **25**, 7036.